

INVESTIGATION OF THE COMBINED USE OF DIESEL AND CNG FUELS ON AN HCCI ENGINE USING RESPONSE SURFACE METHODOLOGY (RSM)

Oğuz Kürşat DEMİRÇİ^{a,*}, Can ÇINAR^b and Tolga KOCAKULAK^c

^{a,*} Erzincan Binali Yıldırım University, Vocational High School, Erzincan, Türkiye

Corresponding author, odemirci@erzincan.edu.tr, +904462266600-43321; ORCID: 0000-0003-1572-2607

^b Gazi University, Faculty of Technology, Department of Automotive Engineering, Ankara, Türkiye

cancinar@gazi.edu.tr; +903122028646; ORCID: 0000-0001-6944-8864

^c Burdur Mehmet Akif Ersoy University, Technical Sciences of High Vocational School, Burdur, Türkiye

tkocakulak@mehmetakif.edu.tr, +902482134555; ORCID: 0000-0002-1269-6370

Abstract: In this study, the effects of the combined use of diesel and compressed natural gas (CNG) fuels on the performance, combustion and emissions were experimentally and statistically investigated in a homogeneous charged compression ignition (HCCI) engine. Diesel and CNG fuels were used at different ratios between 0% and 80% by mass, and tests were conducted at different engine loads. The experimental procedure was designed using the response surface method (RSM) composite central design method. The experimental data were analyzed using MATLAB and entered into the RSM. In order to determine the response parameters predictably, model equations were created, counter graphs were drawn and optimization was carried out. Engine load and CNG ratio, which are the optimum input parameters, were determined as 68.36% and 2.864%, respectively. The response parameter values were obtained as 4.487 bar for IMEP, 39.3% for ITE, 255.5 g/kWh for BSFC, 3.343% for COV_{imep}, 0.247% for CO, 191.566 ppm for HC, 579.538 ppm for NO_x and 1.393 m⁻¹ for smoke. This study, in which a combined diesel and CNG fueled engine operating in HCCI combustion mode is examined with experimental and statistical methods, will fill an important gap in the literature and provide researchers with a new perspective.

Keywords: HCCI engine; Response surface method; Optimization; CNG; Diesel.

1. Introduction

The main power source of motor vehicles today is the internal combustion engine [1,2]. This situation brings with it disadvantageous consequences, such as the dependence on fossil fuels and the increase in emissions and environmental pollution [3]. Thus, improving the fuel consumption and emissions is of great importance for researchers [4,5]. For this purpose, most of the studies in the literature are conducted on alternative fuels and alternative combustion modes on internal combustion engines [6,7].

Internal combustion engines are divided into two classes as compression ignition (CI) and spark ignition (SI) engines [8]. Many structural changes are made and auxiliary systems are used in these engines to improve efficiency and emissions [9,10]. The Atkinson cycle, which is a modified version of the Otto cycle, is used in SI engines in hybrid electric vehicles [11,12]. In parallel with the improvements made in the engine cycles, studies on alternative combustion modes continue. The most popular of these combustion modes are homogeneous charged compression ignition (HCCI), reactivity controlled compression ignition (RCCI) and pre-chamber combustion [13,14].

HCCI is a newly developed combustion mode with high thermal efficiency that simultaneously reduces NO_x and soot emissions [15,16]. In HCCI engines, the fuel-air mixture is homogeneous. There is no need for an additional device to ignite the mixture, and the fuel-air mixture is ignited

spontaneously when it reaches the required ignition temperature as a result of compression [17]. This makes it difficult to control the HCCI combustion mode, torque, speed, lambda, etc. It also narrows the engine operating ranges depending on the parameter values [18]. The increase in CO and UHC emissions is one of the biggest disadvantages of the HCCI engines due to the low temperature combustion [19]. Engines working with HCCI combustion mode allow the use of fuel and fuel mixtures of diesel, gasoline, propane, methanol, butane, compressed natural gas (CNG), hydrogen, etc. [20,21].

The physicochemical properties of the fuels will affect the combustion phase of the HCCI engine. Zhu et al. [15] investigated the mixed fuels formed with different concentrations of diesel and CNG fuels on a CI engine. If the CNG ratio was between 0% and 85%, they did not experience any disturbance in the combustion process. However, if the CNG ratio exceeded 85%, the combustion process was adversely affected. In addition, it has been tried to decrease the maximum pressure by delaying the start of combustion. Improvements were observed in the ratio of soot and UHC by increasing the CNG ratio on the compression ignition engine. Ghaffarzadeha et al. [22] carried out experiments in a reactivity controlled compression ignition (RCCI) engine using diesel/CNG and biodiesel/CNG fuels. With the dual fuel application, they observed significant improvements in both engine performance and emissions at RCCI combustion mode. Aydın [23] investigated the use of CNG fuel on an RCCI engine due to its easy accessibility, low price, and less CO₂, smoke and PM emissions. He used CNG with diesel and safflower biodiesel fuel mixtures at different concentrations. He concluded that the IMEP increased, the combustion time decreased and the NO_x emissions improved with biodiesel and CNG fuels. Feroskhan and coworkers [24] investigated the effects of using biogas and diethyl ether (DEE) on the performance, combustion and emissions of an HCCI engine. They made changes in input parameters such as fuel ratios and engine loads. They observed improvements in thermal efficiency and UHC emissions by reducing the methane concentration. As can be seen from the studies, it is clear that the use of different types of alternative fuels can lead to improvements in the performance, combustion and emission values of SI, CI, RCCI or HCCI combustion engines. Duan et al. [25] carried out experiments with methanol fuel in WTCH and real road driving conditions in a spark-ignition 6-cylinder 4-stroke heavy-duty vehicle. The results obtained using methanol fuel were compared with diesel, diesel-gasoline and CNG fuels. When the results obtained under WHTC conditions are examined, the lowest CO, Non Methane HC, PM and NO_x emission values were obtained when CNG fuel was used. Although the emission values obtained with methanol fuel are slightly higher than those with CNG fuel, they are significantly lower than the results obtained with diesel and diesel-gasoline mixture. When the results obtained from the tests carried out under real road tests are examined, the HC emission value of methanol fuel was obtained to be lower than CNG fueled engine and partially close to diesel fueled engine. When NO_x emissions were examined, the emission values of CNG and diesel fueled engine were higher than methanol fueled engines. The NO_x emission, which was 256 mg/km with methanol fuel, was 2734 mg/km on average in the experiments carried out with CNG fuel, and an average value of 6245 mg/km was obtained with diesel fuel.

However, in the experimental studies, it was seen that too many tests were carried out to determine the results. In addition, it was observed that the results obtained with the experiments were interpreted, but the optimum input parameters that would reach the targeted values for the results were not obtained. Ardebili et al. [26] investigated the use of fusel oil/DEE mixtures on an HCCI engine. They reduced the number of experiments using response surface method (RSM) and created model equations for response parameters. In addition, they determined the optimum input parameters required to reach the targeted response parameters. After their optimization, 41.72% DEE ratio, 884 rpm engine speed and

2.08 lambda ratio values were obtained as the optimum input parameters. They provided the obtained optimization results with a desirability rate of 82%. Ganji and coworkers [27] investigated the effects of compression ratio, injection start and fuel injection pressure on the performance and emissions using RSM. They obtained optimum results of the selected parameters and achieved successful results. The RSM method provides advantages in terms of both time and cost, with a reduction in the number of experiments. It creates models that are used to predict response parameter results based on input parameters. In addition, depending on the targeted response parameters, it plays an important role in determining the optimum input parameter values.

When the literature studies are evaluated, it has been observed that the use of a certain amount of CNG in addition to diesel fuel in a compression ignition engine can lead to improvements in performance, efficiency and emissions. The novelty of this study is that examines the effect on engine performance, combustion and emissions using experimental and RSM methods by using CNG and diesel fuel together on an engine operating with HCCI combustion mode. Within the scope of this study, it is aimed to create a model for the response parameters and optimize them by performing experiments with HCCI engine at different concentrations of CNG and diesel fuels at different engine loads.

2. Materials and methods

In this study, the effects of the use of diesel and CNG fuels on the performance, combustion and emissions in an HCCI engine were experimentally investigated. The experimental set was determined using RSM. Response parameters were calculated with the help of numerical models created in the MATLAB environment, the data obtained as a result of the experiment.

2.1. Test rig

A schematic representation of the test rig is given in Figure 1 [28]. Technical details of the Antor 6 LD 400 single cylinder four-stroke engine used in the experimental study are given in Table 1.

Figure 1. A schematic view of the test rig

Table 1 Technical data of the test engine

Loading of the engine was carried out with a Cussons P8160 brand DC electrical dynamometer. The dynamometer has the capacity to absorb 10 kW of power at 4000 rpm. The determination of the engine crankshaft position was carried out with the help of an encoder with 1000 pulse/revolution sensitivity. A liquid-cooled, AVL 8QP500c model in-cylinder pressure sensor was used to measure in-cylinder pressure. The pressure sensor can measure 0-150 bar with 11.96 pC/bar precision and $\pm 0.6\%$ measurement tolerance. The crankshaft position and in-cylinder pressure values were converted into digital signals by a data acquisition card. The measurement of the diesel fuel consumption was carried out with a Dikomsan JS-B brand precision balance with 1 g sensitivity. The storage pressure of 200 bar CNG tube was reduced to 1 bar with a pressure regulator. CNG was sent to the intake line of the engine. The CNG mass flow rate was adjusted and precisely measured with the help of the Cole-Parmer brand gas flow control device.

A Bosch BEA 350 exhaust gas analyzer and an AVL 4000 DiSmoke smoke measuring device were used to measure engine-out emissions. The smoke measuring device can measure 0%-100% opacity values with 0.1 precision and 0-99.99 m⁻¹ K values with 0.01 precision. The technical data of the Bosch BEA 350 exhaust gas analyzer are given in Table 2.

Table 2 Technical data of the Bosh BEA 350 exhaust gas analyzer

2.2. Test fuels

In the tests, standard diesel and CNG fuels were used in the HCCI mode by controlling them at different concentrations as pure diesel fuel, 40% CNG-60% diesel fuel and 80% CNG-20% diesel fuel. In Table 3, the technical specifications of pure diesel and CNG fuels are given. It is seen that CNG fuel needs more air than diesel fuel for stoichiometric combustion. Although the lower calorific value of CNG is higher than that of diesel fuel, it is seen that its density is almost half.

Table 3 Specifications of the test fuels

Deviations in response parameters may occur depending on the sensitivity of the devices and equipment used in experimental studies [29]. The error rate is obtained by calculating these deviations with uncertainty analysis. The total uncertainty value is defined by Equation 1 [30].

$$Total\ uncertainty = \sqrt{(Torque)^2 + (BSFC)^2 + (IMEP)^2 + (ITE)^2 + (uHC)^2 + (CO)^2 + (NO)^2 + (smoke)^2} \quad (1)$$

Uncertainty values of the response parameters are given in Table 4. In Table 4, the uncertainties of the response parameters are replaced in Equation 1. As a result of the calculation, the error rate of the experimental study was found to be 4.07%.

Table 4 Uncertainty values of performance and emission response parameters

2.3. Numerical analysis

The experimental data were numerically analyzed using MATLAB and the response parameters were obtained. The heat release rate was calculated by entering the crankshaft position and in-cylinder pressure data obtained using experimental methods in Equation 2. In the Equation 2, k is the isentropic coefficient, P is the in-cylinder pressure, V is the cylinder volume, and Q_{heat} is the amount of heat released from the cylinder [31].

$$\frac{dQ}{d\theta} = \frac{k}{k-1} P \frac{dV}{d\theta} + \frac{k}{k-1} V \frac{dP}{d\theta} + \frac{dQ_{heat}}{d\theta} \quad (2)$$

W_{net} is calculated using Equation 3 [32].

$$W_{net} = \int P dV \quad (3)$$

The thermal efficiency was calculated using Equation 4. In this Equation, m indicates mass of diesel and CNG fuels and Q indicates the lower heating value of these fuels [33].

$$\eta_T = \frac{W_{net}}{\dot{m}_{diesel} \times Q_{diesel} + \dot{m}_{CNG} \times Q_{CNG}} \quad (4)$$

It is inevitable to observe differences in in-cylinder pressure data between cycles. To minimize the error occurring in the cycles, the average data of 50 cycles were taken. The cyclical differences were called COV_{imep} and calculated using Equation 5 [34]. X represents the standard deviation, and σ represents the average of the in-cylinder pressure values.

$$COV_{imep} = \frac{\sigma_{imep}}{\bar{X}} \cdot 100 \quad (5)$$

2.4. RSM design

In this study, extrapolation equations, counterplot graphics and optimization for the values of different engine response parameters depending on the ratio of CNG fuel and engine load were performed using the RSM method. The use of RSM was conducted in the Design Expert 11 environment. Box-Behnken design and central composite design (CCD) methods are widely used in RSM [35]. In this study, the experimental set was designed using the CCD method. Two numerical differences were included as variable parameters for the CCD design. The minimum and maximum variable parameter values were determined by evaluating the operating conditions of the engine and are given in Table 5. Because of the created design, it was seen that results should be obtained for 13 different experiments. The design was created for 11 different response values.

Table 5 Independent variables levels

Experiments were carried out according to the desired conditions in the experimental set created by RSM. The data obtained because of the experiments were entered into the RSM interface. Because it gives high regression values, the cubic model was selected as the process order.

3. Results and discussions

The effects of the use of diesel and CNG fuel mixtures in HCCI combustion mode on the combustion, performance, and emissions were determined and a detailed evaluation was made. As response parameters, imep, thermal efficiency, BSFC, COV_{imep} , CA 10, CA 50, combustion duration, CO, UHC, NO_x , and smoke emissions were determined and evaluated.

3.1. ANOVAs

F-value, P-value and remarks were determined for all response parameters and are given in Table 6. F-value and P-value were analyzed depend on the model, engine load and CNG ratio input parameters. The effect of the variable parameters on the response parameters is indicated by the F-value. If the P-value is less than 0.05, it means that the variable parameter is significant for that response parameter [36-38]. In addition, a low P-value indicates a high effect rate. The models appear to be significant for all response parameters. For engine load variable parameters, IMEP, BSFC, COV_{imep} , CO, UHC, NO_x and smoke values are significant, but not significant for other response parameters. For the variable parameters, CNG ratio, thermal efficiency, COV_{imep} , CA50, combustion duration, UHC, NO_x and smoke values are significant, but not significant for other response parameters.

Table 6 ANOVA results

R_2 and adjusted R_2 are used to evaluate the accuracy of statistical results. R_2 , adjusted R_2 , and the difference values between them obtained in this study are given in Table 7. R_2 and adj. The closeness of R_2 values strengthens the accuracy of the statistical study [39, 40].

Table 7 Response R_2 and adj. R_2 value results

3.2. Examination of performance, combustion and emission values

For all response parameters, model equations were created that allow them to be calculated based on different input parameters. Counter graphs were created for all response parameters, and the effect of variable parameters on response parameters was explained in detail.

3.2.1. Indicated mean effective pressure (IMEP)

IMEP is an important parameter in determining and evaluating an engine performance. Equation 6 shows the model used to calculate the IMEP based on different input parameters.

$$IMEP(\text{bar})=5.02+ 1.222A+0.0327B+0.0176AB-0.3403A^2-0.1608B^2+ 0.0585A^2B+0.0649AB^2 \quad (6)$$

The variation of the IMEP with the CNG ratio of the blended fuels and the engine load is given in Figure 2. A continuous increase in IMEP was observed with increasing engine load because of the increase of the amount of fuel and, accordingly, the amount of heat generated by combustion. The temperature increase is caused by the increase of the in-cylinder pressure. It is seen that a maximum pressure of 6.036 bar is obtained under the conditions of 100% engine load and 80% CNG fuel use. Under the same engine load conditions, a slight increase in the imep value was observed when the CNG ratio was 40%. The reason for this is that the combustion start is not delayed more than necessary when the CNG ratio is 40%. In full load conditions, IMEP continuously increased with the increase in the CNG ratio. As the CNG ratio increases, the start of combustion is delayed and the heat generated during the combustion process spreads in the larger cylinder volume, causing a decrease in the pressure increase.

Figure 2. The variation of the imep with the CNG ratio and engine load

3.2.2. Thermal efficiency

The ratio of the chemical energy of the fuel entering the cylinder to the heat energy released as a result of combustion is called thermal efficiency. Equation 7 is used to calculate the thermal efficiency depending on different input parameters.

$$ITE(\%)=0.35 + 0.002A-0.0427B+0.0458AB-0.0325A^2-0.0114B^2+0.017A^2B-0.0033AB^2 \quad (7)$$

The variation of the thermal efficiency with the CNG ratio of the blended fuel and the engine load is given in Figure 3. There was no steady increase or decrease in thermal efficiency with an increase in engine load. However, the thermal efficiency decreases depending on the increase in the engine load in the range of 80% to 100% engine load. It is necessary to send a richer mixture into the cylinder to increase the engine load. In this case, it can be observed that the homogeneity is broken and some of the fuel is thrown out without burning, and a decrease in thermal efficiency can be observed. It is observed that the thermal efficiency decreases continuously with the increase in the CNG ratio. The

auto-ignition temperature of CNG fuel is much higher than diesel fuel. The HCCI engine does not have an extra actuator for combustion control. Because of the increase in the CNG ratio, it is inevitable to increase the auto-ignition value of the blended fuel. Thus, the combustion moves away from the targeted crankshaft angle and causes a corresponding decrease in the thermal efficiency. The highest thermal efficiency was obtained as 39.69% with pure diesel fuel and 62.94% with engine load conditions.

Figure 3. The variation of the ITE with the CNG ratio and engine load

3.2.3. Brake specific fuel consumption (BSFC)

The BSFC was calculated using Equation 8 based on different input parameters.

$$BSFC=248.29-32.425A-0.315B-23.3AB+55.2343A^2+2.59431B^2+25.405A^2B+2.045AB^2 \quad (8)$$

The variation of the BSFC with the CNG ratio of the blended fuels and the engine load is given in Figure 4. It has been determined that there is a significant improvement in the BSFC value when the engine load is between 60% and 90%. It has been determined that the ITE value is also high in this engine load operating range. The reason for this is that the high CA10 and CA50 values are lower between 60% and 90% of engine loads due to the lack of preheating of the engine operating in HCCI mode. Since the lower calorific value of CNG fuel is higher than diesel fuel, a decrease in BSFC is expected. However, depending on the increase in CNG ratio, a serious increase was observed in the BSFC. This is caused by the delay of the ignition time as the CNG value increases and it is thought to cause an increase in the BSFC. The lowest BSFC was obtained as 241.55 g/kWh at 82.62% engine load and 70.29% at CNG ratio conditions.

Figure 4. The variation of the BSFC with the CNG ratio and engine load

3.2.4. COV_{imep}

Equation 9 shows the model used to estimate the COV_{imep} based on different input parameters.

$$COV_{imep}(\%)=9.72+0.7527A + 8.7408B-0.0412AB-2.20898A^2+1.9378B^2-2.8881A^2B-1.0732AB^2 \quad (9)$$

The COV_{imep} variation with the CNG ratio of the blended fuels and the engine load is given in Figure 5. There is no stable increase or decrease in the COV_{imep} depending on the engine load. The significant change in the COV_{imep} value is seen to be CNG as the blended fuel. It is seen that the CNG ratio is 0%, that is, the COV_{imep} value is around 3.2% in the use of pure diesel fuel. It is known that pure diesel fuel ignites more easily than CNG fuel due to its characteristic features such as cetane/octane number and auto-ignition temperature. Easier ignition results in a more balanced operation of the HCCI engine. In this case, it causes a decrease in the differences in pressure values between cycles. The highest COV_{imep} value was obtained as 20.23 bar at 80% CNG fuel mixture ratio and 74.97% engine load conditions.

Figure 5. The variation of the COV_{imep} with the CNG ratio and engine load

3.2.5. CA10 (CA)

Equation 10 shows the model used to estimate the CA10 based on different input parameter values.

$$CA10(CA)=1.24+0.54B-0.81AB+0.8752A^2+1.0552B^2-0.63A^2B+0.45AB^2 \quad (10)$$

The variation of CA10 with the CNG ratio of the blended fuels and the engine load is given in Figure 6. It was observed that there was no stable change in CA10 value with engine load and CNG ratio. The reason for this is that the resistance to self-ignition increases with the increasing CNG ratio, the combustion cannot be carried out regularly and in this case, it leads the engine to work irregularly. It is thought that as the CNG ratio approaches 80%, the CA10 value is shifted, and this is because of the high octane number of the CNG and its resistance to ignition. On the other hand, it is observed that the CA10 increases with the engine load approaching 100%. With the increase of engine load, it is expected that the in-cylinder temperature will increase and accordingly, the ignition onset of HCCI combustion will be brought forward. Since the laminar flame speed of CNG is higher than diesel fuel, gaseous CNG fuel burns faster than liquid diesel fuel. Since the diesel fuel mass is higher in full load mode than in other load positions, delays are observed in the combustion time. As the laminar flame velocity of CNG is higher than diesel fuel, CNG ends the combustion phase faster than diesel fuel [41].

Figure 6. The variation of the CA10 with the CNG ratio and engine load

3.2.6. CA50 (CA)

In internal combustion engines, the crank angle at which 50% of the cumulative heat dissipation occurs is called CA50 [42]. Equation 11 shows the model used to estimate the CA50 based on different input parameter values.

$$CA50(CA)=15.8+0.9A-1.98B-1.44AB+1.2103A^2+1.5703B^2-0.18A^2B+0.36AB^2 \quad (11)$$

The variation of the CA50 with the CNG ratio of the blended fuels and the engine load is given in Figure 7. The CA50 value was increased with the increase of the engine load ratio. It was stated that the increase in the CNG ratio delayed the start of combustion. However, the CA50 value delayed with the increase of CNG ratio. This is caused by the higher laminar flame velocity of CNG compared to diesel fuel. The highest CA50 was calculated as 23.24 CA using pure diesel fuel at full load. It was concluded that the lowest CA50 was 15.17 CA at 62.79% CNG ratio and 71.67% at engine load.

Figure 7. The variation of the CA50 with the CNG ratio and engine load

3.2.7. Combustion duration (CA)

The combustion duration is expressed as the value of CA passing between CA10 and CA90 [43]. Equation 12 shows the model used to estimate the combustion duration based on different input parameters.

$$CD(CA)=59.26+7.92A-9.9B-2.88AB+5.3379A^2+4.0779B^2-0.54A^2B-3.24AB^2 \quad (12)$$

The variation of the combustion duration with the CNG ratio and engine load is given in Figure 8. The combustion duration decreased with the CNG ratio increased. Although the octane number and auto-ignition temperature of CNG fuel are high, the laminar flame velocity is also high [44]. Although the initial ignition time delays with the increase in the CNG fuel ratio, it can complete the combustion process in a shorter time after ignition. It is seen that the minimum combustion duration value was

obtained with a CA of 53.46, a CNG ratio of 66.54%, and an engine load ratio of 61.66%. The maximum combustion value was determined as 86.28 CA in pure diesel fuel and full load condition. It was obtained that the increase of engine load increased the combustion duration.

Figure 8. The variation of the combustion duration with the CNG ratio and engine load

3.2.8. Carbon monoxide emissions (%)

The CO emissions was calculated depend on different input parameters using Equation 13.

$$CO(\%)=0.29+0.2865A-0.12B-0.439AB+0.1924A^2+0.0429B^2-0.2755A^2B+0.174AB^2 \quad (13)$$

The variation of the CO emissions with the CNG ratio and load is given in Figure 9. CO emissions are caused by the low combustion temperatures, the inhomogeneity of the mixture, and the lack of oxygen. As the load increases, it is expected that the CO emissions will improve as the combustion end temperature increases. However, a continuous increase in the CO emissions were observed with increasing engine load. Because to increase the engine load the quantity of fuel sent into the cylinder is increased and this is caused the oxygen deficiency. Improvements were observed in CO emissions with the increase in the CNG ratio. It is thought that the reason for this may be that CNG fuel contains less carbon than diesel fuel. In addition, due to the low density of CNG fuel, it provides support to obtain a more homogeneous mixture. This helps to dampen the homogeneity problem, which is one of the biggest criteria of CO formation.

Figure 9. The variation of the CO with the CNG ratio and engine load

3.2.9. Unburned hydrocarbon emissions (ppm)

Equation 14 shows the model used to estimate the UHC based on different input parameters.

$$UHC(\text{ppm})=297.76-47.5A+90.5B-71.5AB-6.1551A^2-7.1551B^2+32A^2B+37AB^2 \quad (14)$$

The variation of the UHC emissions with the CNG ratio of the mixed fuel and the engine load is given in Figure 10. The formation of UHC emissions is caused by low combustion end temperature, excess fuel and the inability to obtain a homogeneous mixture. It is expected that the UHC emissions will decrease depending on the engine load. UHC emissions increased with the increase of CNG ratio. It is thought that the reason for this is the need for more air due to the excess stoichiometric air/fuel mixing ratio value of the CNG fuel. It was observed that the maximum UHC emission was 498 ppm, at 50% engine torque and 80% engine load.

Figure 10. The variation of the UHC with the CNG ratio and engine load

3.2.10. NO_x emissions (ppm)

Equation 15 shows the model used to estimate the NO_x based on different input parameters.

$$NO_x(\text{ppm})=699.38+141A+109.5B+115.75AB-56.3276A^2-1.8276B^2-6.75A^2B+18.25AB^2 \quad (15)$$

The variation of NO_x emissions with the CNG ratio of the blended fuel and the engine load is given in Figure 11. The main causes of NO_x emission are high end-of-combustion temperature and inhomogeneous fuel-air mixture [45]. The highest NO_x emission was 1036 ppm with 80% CNG ratio

and full load conditions. An increase in NO_x was observed with increasing engine load. With the increase in engine load, the increase in the combustion end temperature is inevitable, which triggers the formation of NO_x emissions. NO_x emissions increased depending on the increase in engine load and CNG ratio. This increase is caused by the slight increase of the temperature at the end of the combustion due to the high lower calorific value of the CNG.

Figure 11. The variation of the NO_x with the CNG ratio and engine load

3.2.11. Smoke

Equation 16 shows the model used to estimate the smoke based on different input parameters.

$$\text{Smoke}(m^{-1})=0.422+0.665A-1.025B-1.1275AB+0.2865A^2+0.6465B^2-0.2225A^2B+0.5225AB^2 \quad (16)$$

The variation of the smoke emissions with the CNG ratio and engine load is given in Figure 12. HCCI engines operate continuously with a lean mixture [46]. However, if the amount of fuel is increased to increase the engine loads, there is a decrease in the lambda value. In this case, it is inevitable that smoke emissions will increase [47]. The increase in engine load also causes to increase the smoke K-factor. This is thought to be due to the enrichment of the mixture at high engine loads. A decrease in the smoke K-factor was observed with the increase in the CNG ratio. Wategavea et al. have reduced the smoke emissions to almost zero by using CNG instead of using biodiesel on the engine operating in RCCI mode [48].

Figure 12. The variation of the smoke with the CNG ratio and engine load

3.3. Comparison of experimental results and statistical results

Consistency of experimental and statistical results increases the reliability of the study. In order to meet these results, parts containing the data belonging to the answers and preserved can be created. In this study, these graphics were created in the Design expert environment. Figure 13 and Figure 14 show the comparison of actual and predicted results for the response parameters used in the Optimization. The results for IMEP, ITE, COV_{imep} and BSFC are shown in Figure 13. For COV_{imep} and BSFC response parameters, there is almost no difference between the estimated and actual values. There are negligible differences between the limits of the IMEP and ITE response parameters.

Figure 13. Comparison of experimental and statistical results for IMEP, ITE, COV_{imep} , BSFC

The results for CO, UHC, NO_x and Smoke are presented in Figure 14. It is clearly seen that there is no difference between the estimated and actual values for the Smoke response parameter. Acceptable deviations are observed for CO, UHC and NO_x parameters. It is seen that the actual and estimated values are close to each other. This situation strengthens the reliability of the data obtained by the statistical study.

Figure 14. Comparison of experimental and statistical results for CO, UHC, NO_x , Smoke

3.4. Optimization

RSM optimization module was used to determine the optimum input parameters to obtain the targeted response parameters. The input parameters to be optimized are the engine torque ratio and the CNG ratio taken throughout the run. During the optimization process, it was aimed to have the IMEP and ITE values at the maximum, the BSFC, CO, NO_x, UHC and smoke values at the minimum, and the COV_{imep} value within a certain range. The target value for CA10 and combustion duration response parameters was not included because there was no target value. As a result of the experiments, it was determined that the CA50 value was between 15.48 and 23.04 °CA. CA50 minimum and maximum values could not be included in the optimization because they were within the targeted range of 7-11 °CA. After the optimization, IMEP, ITE, BSFC, COV_{imep}, CA10, CA50, combustion duration, CO, HC, NO_x and smoke values were determined. Input and response parameters used in the optimization are shown in Table 8.

Table 8 Optimization parameters and results

The optimum variable parameter values were found to be Engine load 68.364 Nm and CNG ratio 2.864%. In the study, optimization was carried out depending on combustion, performance and emission response parameters. When evaluated individually, it is clearly seen that the CNG ratio has a large effect on each response parameter. Negative effects on some performance and combustion parameters have been observed with the use of CNG and the reasons are clearly stated. As a result of optimization, the best targets were determined for each response parameter. For this reason, it is thought that a low CNG value is obtained after optimization.

In order to evaluate the accuracy and reliability of the optimization, the desirability value must be high [49]. Desirability value being close to 1 indicates closeness to reaching the targeted value [50]. In the graph in Figure 15, there are input parameters, response parameters, and desirability values calculated together. The combined desirability value was determined as 0.7792, which strengthens the reliability of the optimization.

Figure 15. Desirability rate of optimization

4. Conclusion

In this study, the effects of using standard diesel and CNG fuels on combustion, performance, and emissions were experimentally and statistically investigated in an HCCI engine. The results of this study, which will give researchers a new perspective, will make a significant contribution to the literature. The following results were obtained;

- With the increase in CNG ratio, BSFC, COV_{imep}, UHC and NO_x values increased; ITE, CA50, combustion duration, CA and smoke values decrease; and unstable behavior was detected in imep and CA10 values.
- With the increase in engine load, IMEP, CA50, combustion duration, CO, NO_x and smoke increased, ITE and BSFC decreased; and unstable behavior was observed in COV_{imep}, CA10 and UHC values.
- After the optimization, the combined desirability ratio was obtained as 0.779. Among the optimum input parameters, engine load was determined as 68.36% and CNG ratio as 2.864%.
- The response parameter values were obtained as 4.487 bar for IMEP, 39.3% for indicated thermal efficiency, 255.5 g/kWh for BSFC, 3.343% for COV_{imep}, 1.45 °CA for CA10, 18.415°CA for CA50,

70 °CA for combustion duration, 0.247% for CO, 191.566 ppm for HC, 579.538 ppm for NO_x and 1.393 m-1 for smoke.

- It can be concluded that the use of CNG on the HCCI engine delays the CA10 and CA50 more than desired, and accordingly, disadvantageous situations occur in many response parameters.
- It is recommended to include the CA50 within the targeted values by using preheating on the system, in order to improve combustion, performance, and emissions.

Nomenclature

Biographies

Oğuz Kürşat Demirci received PhD degree from the Automotive Engineering Department of Gazi University, Türkiye, in 2021. He works as a Lecturer in the Machine Programme at Erzincan Binali Yıldırım University. His main research areas are on internal combustion engines, alternative fuels, emissions, HCCI engines.

Can Çınar received PhD degree from the Mechanical Education Department of Gazi University, Türkiye, in 2001. He works as a professor in the Automotive Engineering Department of Gazi University. His main research areas are on internal combustion engines, thermal systems, thermal machines, differential equations, numerical analysis, engineering and technology.

Tolga Kocakulak received MSc degree from the Automotive Engineering Department of Gazi University, Türkiye, in 2019. He works as a Lecturer in the Hybrid and Electric Vehicles Technology Programme at Burdur Mehmet Akif University. His main research areas are on internal combustion engines, fuel cells, hybrid vehicles, response surface methods.

References

1. Yu, C., Deng, Y., Qin, Z., et al. "Traffic volume and road network structure: Revealing transportation-related factors on PM2.5 concentrations", *Transportation Research Part D: Transport and Environment*, **124**, 103935, pp. 1-19 (2023) <https://doi.org/10.1016/j.trd.2023.103935>.
2. Bhan, S., Gautam, R. and Singh, P. "An experimental assessment of combustion, emission, and performance behavior of a diesel engine fueled with newly developed biofuel blend of two distinct waste cooking oils and metallic nano-particle (Al₂O₃)", *Scientia Iranica*, **29**(4), pp. 1853-1867 (2022) <https://doi.org/10.24200/sci.2022.58882.5947>.
3. Duan, X., Lai, MC., Jansons, M., et al. "A review of controlling strategies of the ignition timing and combustion phase in homogeneous charge compression ignition (HCCI) engine", *Fuel*, **285**, 119142, pp. 1-24 (2021) <https://doi.org/10.1016/j.fuel.2020.119142>.
4. Arabaci, E., İcingür, Y., Solmaz, H., et al. "Experimental investigation of the effects of direct water injection parameters on engine performance in a six-stroke engine", *Energy Conversion and Management*, **98**, pp. 89-97 (2015) <https://doi.org/10.1016/j.enconman.2015.03.045>.
5. Demirci, O.K., Uyumaz, A., Sarıdemir, S., et al. "Performance and emission characteristics of a Miller cycle engine" *International Journal of Automotive Engineering and Technologies*, **7**(3), pp. 107-116 (2018) <https://doi.org/10.18245/ijaet.486408>.
6. Awais, M., "Deposition of anti-stick coatings to prevent hydrocarbon buildup on truck engines" *Scientia Iranica*, **27**(5), pp. 2489-2497 (2020) <https://doi.org/10.24200/SCI.2020.53021.3014>.
7. Köse, S., Babagiray, M. and Kocakulak, T. "Response surface method based optimization of the viscosity of waste cooking oil biodiesel", *Engineering Perspective*, **1**(1), pp. 30-37 (2021) <http://dx.doi.org/10.29228/sciperspective.49697>.

8. Kirbaş, İ. and Kocakulak, T. “Determination of Burdur province carbon footprint”, *Dokuz Eylül University Faculty of Engineering Journal of Science and Engineering*, **24**(70), pp. 317-327 (2022) <https://doi.org/10.21205/deufmd.2022247028>.
9. Guo, Q., Liu, J., Wu, B., et al. “On the optimization of the double-layer combustion chamber with and without EGR of a diesel engine” *Energy*, **247**, 123486, pp. 1-14 (2022) <https://doi.org/10.1016/j.energy.2022.123486>.
10. Praveena, V., Martin, M.L.J. and Geo, V.E. “Combined effects of various strategies to curtail exhaust emissions in a biomass waste fueled CI engine coupled with SCR system”, *Engineering Science and Technology, an International Journal*, **33**, 101085 (2022) <https://doi.org/10.1016/j.jestch.2021.101085>.
11. Li, Y., Wang, S., Duan, X., et al. “Multi-objective energy management for Atkinson cycle engine and series hybrid electric vehicle based on evolutionary NSGA-II algorithm using digital twins”, *Energy Conversion and Management*, **230**, 113788 (2021) <https://doi.org/10.1016/j.enconman.2020.113788>.
12. Niu, Q., Sun, B., Zhang, D., et al. “Research on performance optimization and fuel-saving mechanism of an Atkinson cycle gasoline engine at low speed and part load”, *Fuel*, **265**, 117010 (2020) <https://doi.org/10.1016/j.fuel.2020.117010>.
13. Gharehghani, A., Kakoei, A., Andwari, A.M., et al. “Numerical investigation of an rcci engine fueled with natural gas/dimethyl-ether in various injection strategies”, *Energies*, **14**(6), 1638 (2021) <https://doi.org/10.3390/en14061638>.
14. Salahi, M.M. and Gharehghani, A. “Control of combustion phasing and operating range extension of natural gas PCCI engines using ozone species”, *Energy Conversion and Management*, **199**, 112000 (2019) <https://doi.org/10.1016/j.enconman.2019.112000>.
15. Zhu, Z., Li, Y. and Shi, C. “Effect of natural gas energy fractions on combustion performance and emission characteristics in an optical CI engine fueled with natural gas/diesel dual-fuel”, *Fuel*, **307**, 121842 (2022) <https://doi.org/10.1016/j.fuel.2021.121842>.
16. Verma, S.K., Gaur, S., Akram, T., et al. “Emissions from homogeneous charge compression ignition (HCCI) engine using different fuels: a review”, *Environmental Science and Pollution Research*, **29**, pp. 5960-5969 (2022) <https://doi.org/10.1007/s11356-021-15602-x>.
17. Mofijur, M., Hasan, M.M., Mahlia, T.M.I., et al. “Performance and emission parameters of homogeneous charge compression ignition (HCCI) engine: a review”, *Energies*, **12**(18), 3557 (2019) <https://doi.org/10.3390/en12183557>.
18. Polat, S., Yücesu, H.S., Kannan, K., et al. “Experimental comparison of different injection timings in an HCCI engine fueled with n-heptane”, *International Journal of Automotive Science and Technology*, **1**(1), pp. 1-6 (2017) Retrieved from <https://dergipark.org.tr/en/pub/ijastech/issue/26816/288015>.
19. Calam, A., Solmaz, H., Yılmaz, E., et al. “Investigation of effect of compression ratio on combustion and exhaust emissions in A HCCI engine”, *Energy*, **168**, pp. 1208-1216. (2019) <https://doi.org/10.1016/j.energy.2018.12.023>.
20. Çelebi, S., Haşımoğlu, C., Uyumaz, A., et al. “Operating range, combustion, performance and emissions of an HCCI engine fueled with naphtha”, *Fuel*, **283**, 118828 (2021) <https://doi.org/10.1016/j.fuel.2020.118828>.
21. Ardebili, S.M.S., Nacak, Ç., Kocakulak, T., et al. “Experimental investigation and optimization of HCCI engine fueled by isopropanol and heptane mixture”, *Engineering Perspective*, **1**(2), pp. 63-78 (2021) <http://dx.doi.org/10.29228/eng.pers.51253>.
22. Ghaffarzadeh, S., Toosi, A.N. and Hosseini, V. “An experimental study on low temperature combustion in a light duty engine fueled with diesel/CNG and biodiesel/CNG”, *Fuel*, **262**, 116495 (2020) <https://doi.org/10.1016/j.fuel.2019.116495>.
23. Aydın, H., “An innovative research on variable compression ratio in RCCI strategy on a power generator diesel engine using CNG-safflower biodiesel”, *Energy*, **231**, 121002 (2021) <https://doi.org/10.1016/j.energy.2021.121002>.
24. Feroskhan, M., Thangavel, V., Subramanian, B., et al. “Effects of operating parameters on the performance, emission and combustion indices of a biogas fuelled HCCI engine”, *Fuel*, **298**, 120799 (2021) <https://doi.org/10.1016/j.fuel.2021.120799>.
25. Duan, X., Feng, L., Liu, H., et al. “Experimental investigation on exhaust emissions of a heavy-duty vehicle powered by a methanol-fuelled spark ignition engine under world Harmonized Transient Cycle and actual on-road driving conditions”, *Energy*, **282**, 128869 (2023) <https://doi.org/10.1016/j.energy.2023.128869>.

26. Ardebili, S.M.S., Solmaz, H., Calam, A., et al. "Modelling of performance, emission, and combustion of an HCCI engine fueled with fusel oil-diethylether fuel blends as a renewable fuel", *Fuel*, **290**, 120017 (2021) <https://doi.org/10.1016/j.fuel.2020.120017>.
27. Ganji, P.R., Chintala, K.P., Raju, V.R., et al. "Parametric study and optimization using RSM of DI diesel engine for lower emissions", *Journal of the Brazilian Society of Mechanical Sciences and Engineering*, **39**(3), pp. 671-680 (2017) <https://doi.org/10.1007/s40430-016-0600-0>.
28. Demirci, O.K. "The investigation of the effects of using CNG on engine performance emissions and combustion in an HCCI engine", PhD Thesis, *Graduate School of Natural and Applied Sciences*, Gazi University, Ankara (2021).
29. Ganesan, N., Sahoo, B. B., Ekambaram, P., et al. "Experimental based comparative exergy analysis of a spark- ignition Honda GX270 Genset engine fueled with LPG and syngas", *Energy Science & Engineering*, **10**(7), pp. 2191-2204 (2022) <https://doi.org/10.1002/ese3.1125>.
30. Kadian, A. K., Khan, M. and Sharma, R. P. "Performance enhancement and emissions mitigation of DI-CI engine fuelled with ternary blends of jatropha biodiesel-diesel-heptanol", *Materials Science for Energy Technologies*, **5**, pp. 145-154 (2022) <https://doi.org/10.1016/j.mset.2022.01.002>.
31. Polat, S., Solmaz, H., Yılmaz, E., et al. "Mapping of an HCCI engine using negative valve overlap strategy", *Energy Sources, Part A: Recovery, Utilization, and Environmental Effects*, **42**(9), pp. 1140-1154 (2020) <https://doi.org/10.1080/15567036.2019.1602224>.
32. Uyaroglu, A., Guri, M., Kocakulak, T., et al. "Combustion, performance and emission analyses of organic manganese-added crambe abyssinica biodiesel in a direct injection diesel engine", *Fuel*, **297**, 120770 (2021) <https://doi.org/10.1016/j.fuel.2021.120770>.
33. Arabacı, E. "Simulation and performance analysis of a spark ignition engine using gasoline and LPG as fuel", *Journal of the Faculty of Engineering and Architecture of Gazi University*, **36**(1), pp. 447-457 (2021) <https://doi.org/10.17341/gazimmfd.561583>.
34. Polat, S., Solmaz, H., Calam, A., et al. "Estimation of the COVIMEP variation in a HCCI Engine" *Journal of Polytechnic*, **23**(3), pp. 721-727 (2020) <https://doi.org/10.2339/politeknik.567865>.
35. Oza, S., Kodgire, P. and Kachhwaha, S.S. "Analysis of RSM based BBD and CCD techniques applied for biodiesel production from waste cotton-seed cooking oil via ultrasound method", *Analytical Chemistry Letters*, **12**(1), 86-101 (2022) <https://doi.org/10.1080/22297928.2021.2019611>.
36. Babagiray, M., Kocakulak, T., Ardebili, S.M.S., et al. "Experimental and statistical investigation of different valve lifts on HCCI combustion, performance and exhaust emissions using response surface method", *Energy*, **244**, pp. 1-15, 123184 (2022) <https://doi.org/10.1016/j.energy.2022.123184>.
37. Perec, A. "Multiple response optimization of abrasive water jet cutting process using response surface methodology (RSM)", *Procedia Computer Science*, **192**, pp. 931-940 (2021) <https://doi.org/10.1016/j.procs.2021.08.096>.
38. Astutiningsih, F., Anggrahini, S., Fitriani, A., et al. "Optimization of saffron essential oil nanoparticles using chitosan-Arabic gum complex nanocarrier with ionic gelation method", *International Journal of Food Science*, 4035033, pp. 1-14 (2022) <https://doi.org/10.1155/2022/4035033>.
39. Baloyi, N.P., Nseke, J.M. and Makhatha, M. E. "Application of response surface methodology (RSM) for simultaneous optimization of kinetic parameters affecting gold leaching in thiosulfate based media: a statistical approach", *Journal of Chemistry*, 8348167, pp. 1-11 (2022) <https://doi.org/10.1155/2022/8348167>.
40. Ali, M., Kumar, A., Yvaz, A., et al. "Central composite design application in the optimization of the effect of pumice stone on lightweight concrete properties using RSM", *Case Studies in Construction Materials*, **18**(e01958), pp. 1-20 (2023) <https://doi.org/10.1016/j.cscm.2023.e01958>.
41. Abdelaal, M.M. and Hegab, A.H. "Combustion and emission characteristics of a natural gas-fueled diesel engine with EGR", *Energy Conversion and Management*, **64**, pp. 301-312 (2012) <https://doi.org/10.1016/j.enconman.2012.05.021>.
42. Solmaz, H., Calam, A., Halis, S., et al. "Investigation of the effects of intake manifold pressure on performance and combustion characteristics in an HCCI engine", *Journal of the Faculty of Engineering and Architecture of Gazi University*, **37**(4), pp. 1735-1749 (2022) <https://doi.org/10.17341/gazimmfd.602742>.
43. Zarrinkolah, M.T. and Hosseini, V. "Detailed analysis of the effects of biodiesel fraction increase on the combustion stability and characteristics of a reactivity-controlled compression ignition diesel-biodiesel/natural gas engine", *Energies*, **15**(3), pp. 1-17 (2022) <https://doi.org/10.3390/en15031094>.

44. Kafle, S., Kalwar, A., Valera, H., et al. "Compressed natural gas utilization in dual-fuel internal combustion engines", *Advanced Combustion for Sustainable Transport*, Springer, Singapore, pp. 273-296 (2022) https://doi.org/10.1007/978-981-16-8418-0_9.
45. Zhao, W., Fan, W. and Zhang, R. "Study on the effect of fuel injection on combustion performance and NO_x emission of RQL trapped-vortex combustor", *Energy Reports*, **9**(6), pp. 54-63 (2023) <https://doi.org/10.1016/j.egy.2023.04.028>.
46. Godiño, J.A.V., García, M.T. and Aguilar, F.J.J.E. "Experimental analysis of late direct injection combustion mode in a compression-ignition engine fuelled with biodiesel/diesel blends", *Energy*, **239**(Part A), 121895, pp. 1-13 (2022) <https://doi.org/10.1016/j.energy.2021.121895>.
47. Nalla, B.T., Devarajan, Y., Subbiah, G. et al. "Investigations of combustion, performance, and emission characteristics in a diesel engine fueled with Prunus domestica methyl ester and n-butanol blends", *Environmental Progress & Sustainable Energy*, **41**(4), e13811, pp. 1-8 (2022) <https://doi.org/10.1002/ep.13811>.
48. Wategave, S.P., Banapurmath, N.R., Sawant, M.S., et al. "Clean combustion and emissions strategy using reactivity controlled compression ignition (RCCI) mode engine powered with CNG-Karanja biodiesel", *Journal of the Taiwan Institute of Chemical Engineers*, **124**, pp. 116-131 (2021) <https://doi.org/10.1016/j.jtice.2021.04.055>.
49. Nawaz, A., Atif, M., Khan, A., et al. "Solar light driven degradation of textile dye contaminants for wastewater treatment—studies of novel polycationic selenide photocatalyst and process optimization by response surface methodology desirability factor", *Chemosphere*, **328**, 138476 (2023) <https://doi.org/10.1016/j.chemosphere.2023.138476>.
50. Percy, A. J. and Edwin, M. "Studies on the performance and emission characteristics of a dual fuel VCR engine using producer gas as secondary fuel: An optimization approach using response surface methodology", *Energy*, **263**, 125685, pp. 1-18 (2023) <https://doi.org/10.1016/j.energy.2022.125685>.

Figure Titles

- Figure 1. A schematic view of the test rig
- Figure 2. The variation of the imep with the CNG ratio and engine load
- Figure 3. The variation of the ITE with the CNG ratio and engine load
- Figure 4. The variation of the BSFC with the CNG ratio and engine load
- Figure 5. The variation of the COV_{imep} with the CNG ratio and engine load
- Figure 6. The variation of the CA10 with the CNG ratio and engine load
- Figure 7. The variation of the CA50 with the CNG ratio and engine load
- Figure 8. The variation of the combustion duration with the CNG ratio and engine load
- Figure 9. The variation of the CO with the CNG ratio and engine load
- Figure 10. The variation of the UHC with the CNG ratio and engine load
- Figure 11. The variation of the NO_x with the CNG ratio and engine load
- Figure 12. The variation of the smoke with the CNG ratio and engine load
- Figure 13. Comparison of experimental and statistical results for IMEP, ITE, COV_{imep}, BSFC
- Figure 14. Comparison of experimental and statistical results for CO, UHC, NO_x, Smoke
- Figure 15. Desirability rate of optimization

Table Titles

- Table 1 Technical data of the test engine
- Table 2 Technical data of the Bosh BEA 350 exhaust gas analyzer
- Table 3 Specifications of the test fuels
- Table 4 Uncertainty values of performance and emission response parameters
- Table 5 Independent variables levels
- Table 6 ANOVA results
- Table 7 Response R² and adj. R² value results
- Table 8 Optimization parameters and results

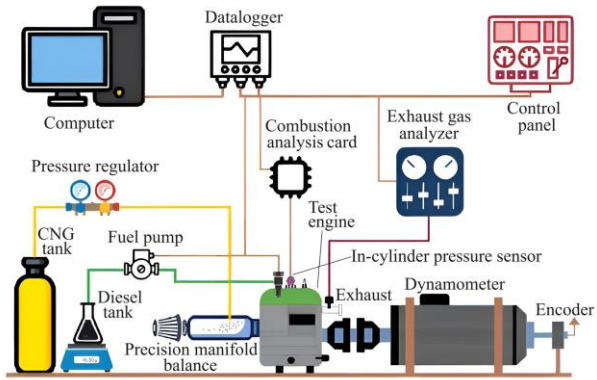


Figure 1. A schematic view of the test rig

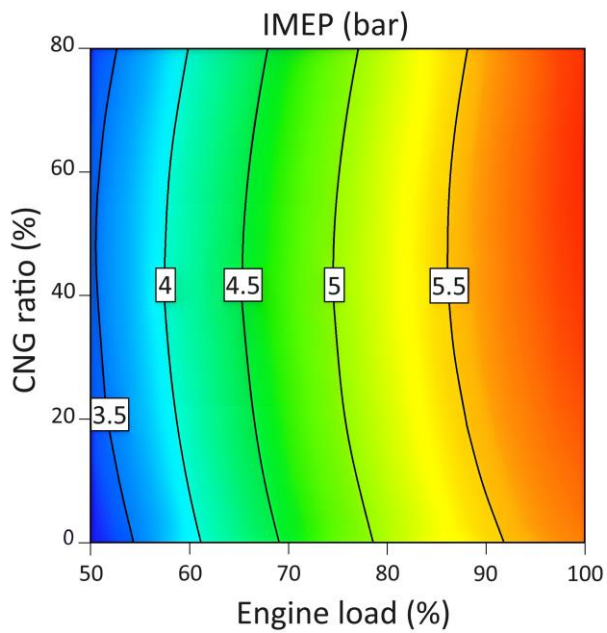


Figure 2. The variation of the imep with the CNG ratio and engine load

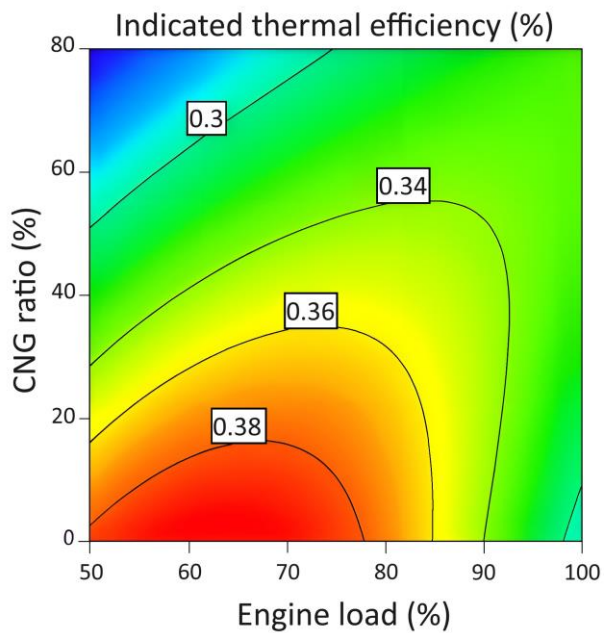


Figure 3. The variation of the ITE with the CNG ratio and engine load

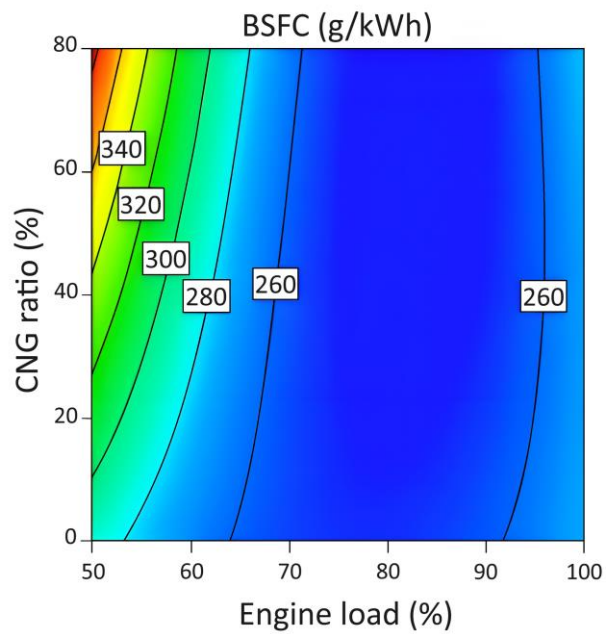


Figure 4. The variation of the BSFC with the CNG ratio and engine load

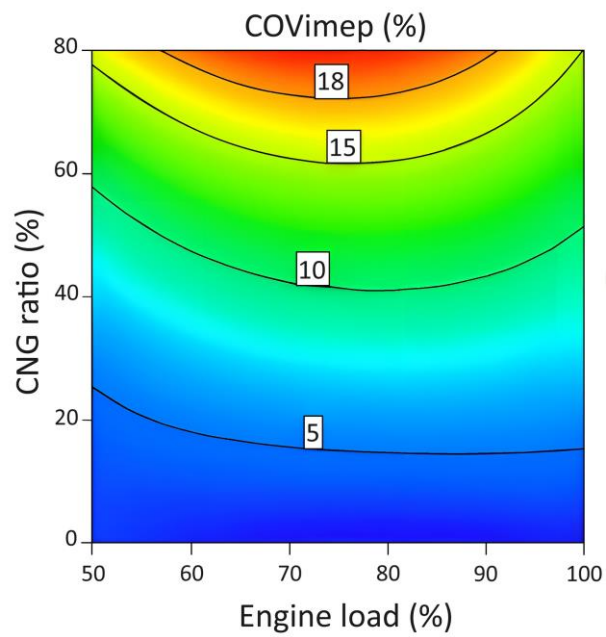


Figure 5. The variation of the COVimep with the CNG ratio and engine load

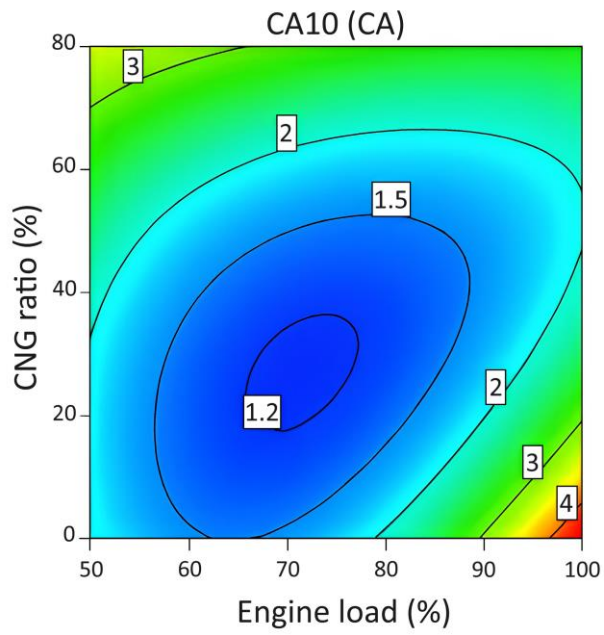


Figure 6. The variation of the CA10 with the CNG ratio and engine load

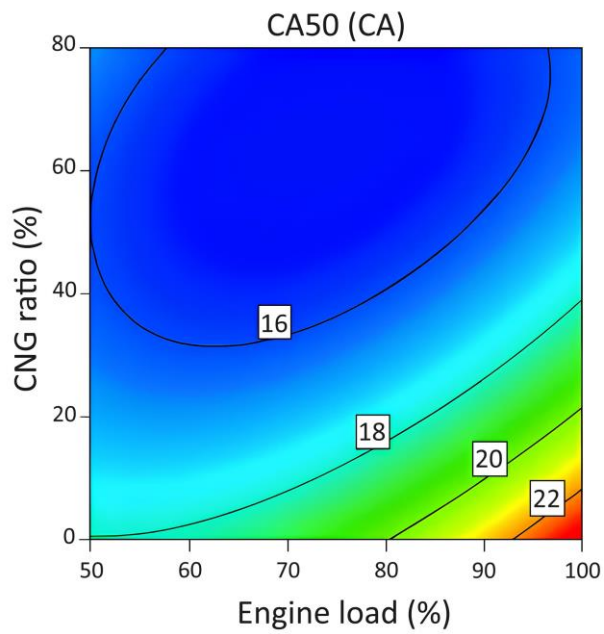


Figure 7. The variation of the CA50 with the CNG ratio and engine load

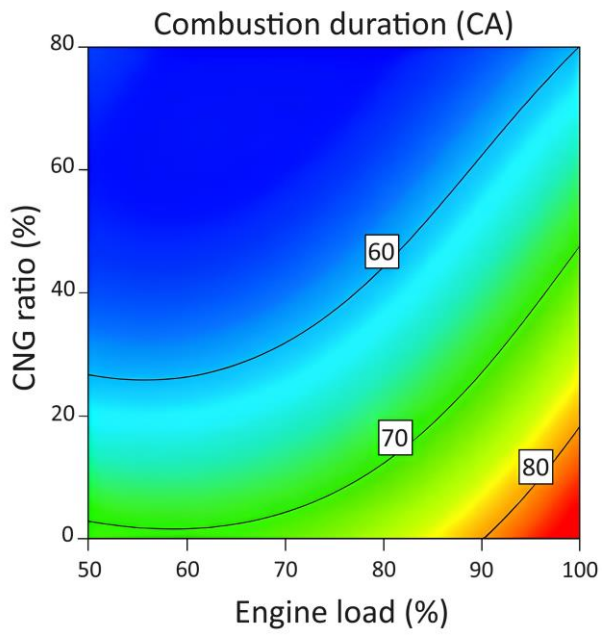


Figure 8. The variation of the combustion duration with the CNG ratio and engine load

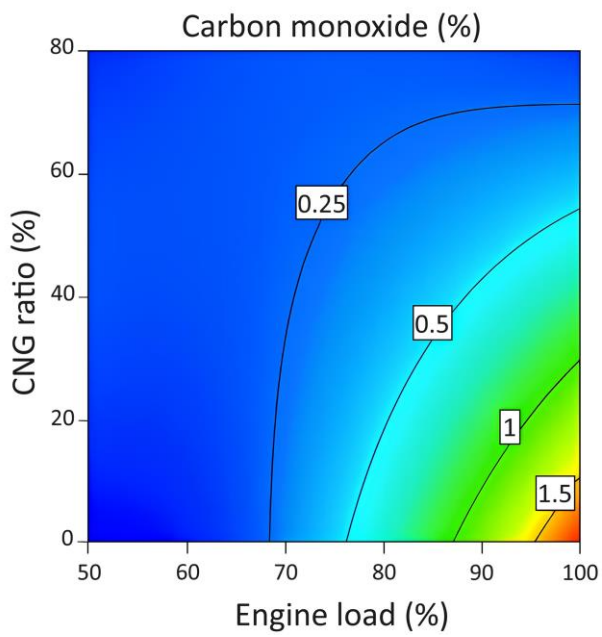


Figure 9. The variation of the CO with the CNG ratio and engine load

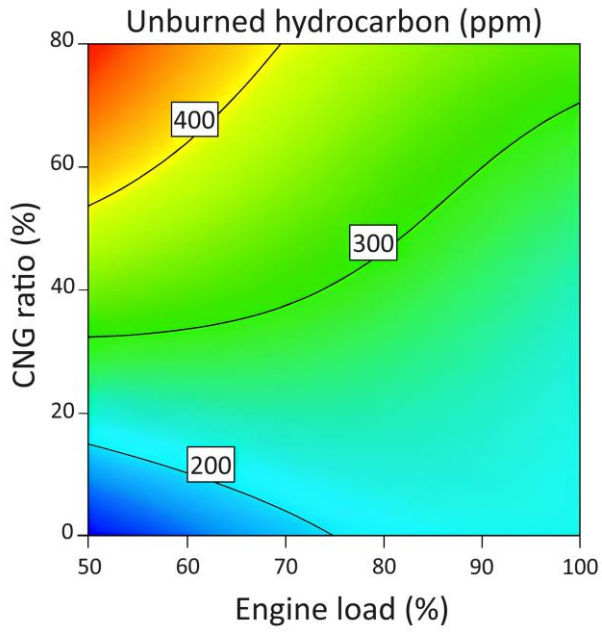


Figure 10. The variation of the UHC with the CNG ratio and engine load

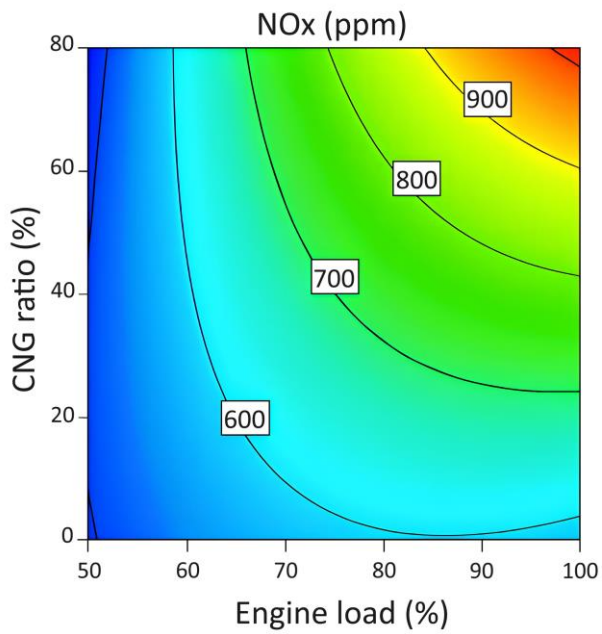


Figure 11. The variation of the NOx with the CNG ratio and engine load

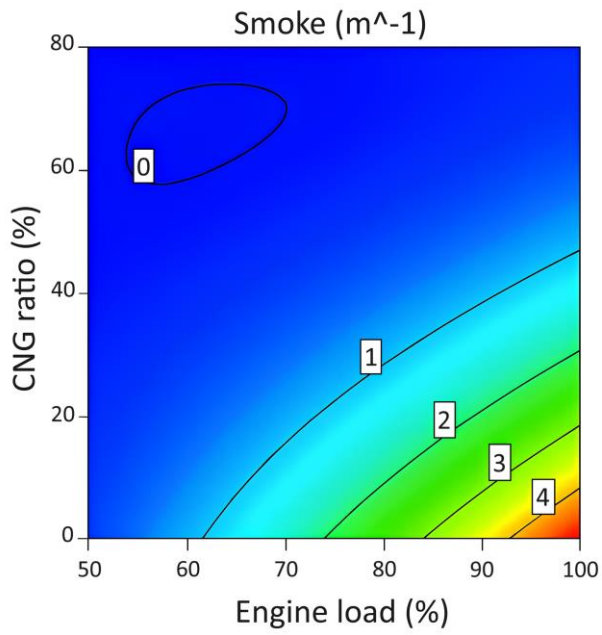


Figure 12. The variation of the smoke with the CNG ratio and engine load

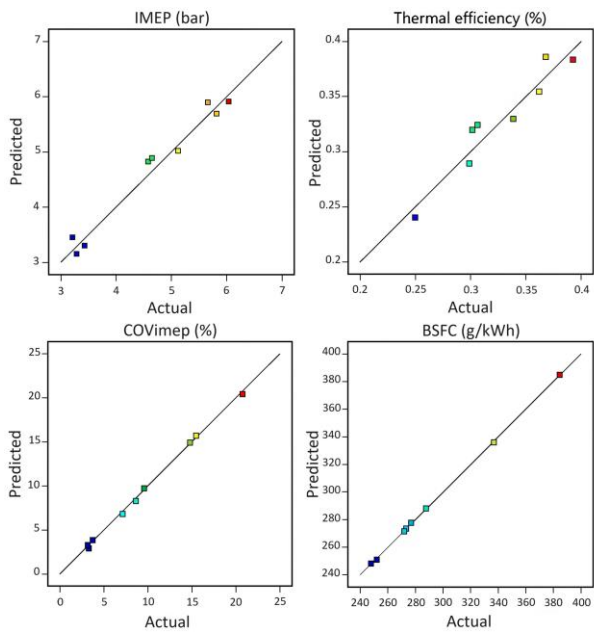


Figure 13. Comparison of experimental and statistical results for IMEP, ITE, COVimep, BSFC

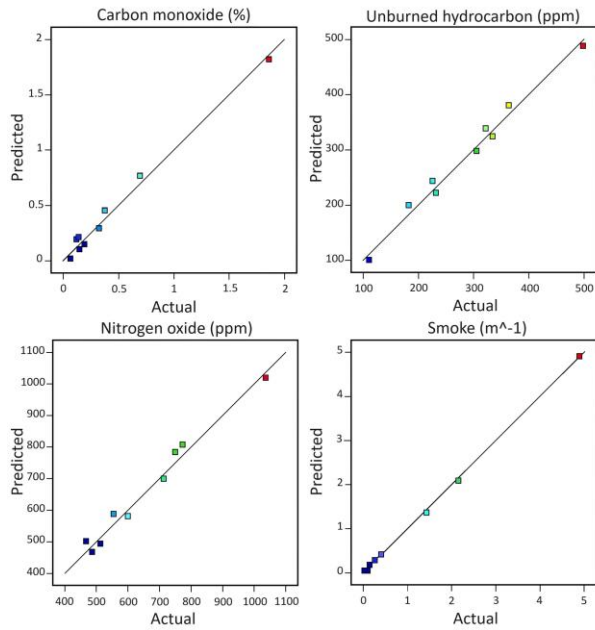


Figure 14. Comparison of experimental and statistical results for CO, UHC, NO_x, Smoke

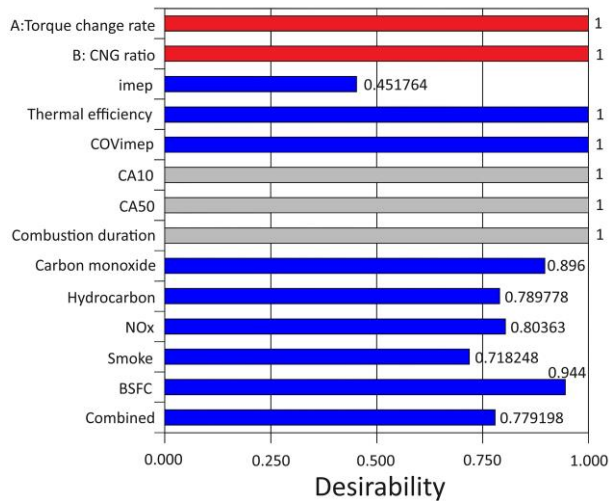


Figure 15. Desirability rate of optimization

Table 1 Technical data of the test engine

Brand-Model	6LD 400
Bore x Stroke	86 mm x 68 mm
Compression ratio	18:1
Maximum power	5.4 kW @ 3000 rpm
Maximum torque	19.6 Nm @ 2200 rpm
Maximum speed	3600 rpm
Injection pressure/time	180 bar/24°CA
Injector hole number/diameter	4 x 0.24mm
Injector tip angle	160°

Table 2 Technical data of the Bosh BEA 350 exhaust gas analyzer

	Range	Sensitivity
CO (%)	0 – 10	0.001
UHC (ppm)	0 – 9999	1
NO _x (ppm)	0 – 5000	1

O ₂	0 – 22	0.01
CO ₂ (%)	0 – 18	0.01
Lambda	0.5 – 9.9999	0.001

Table 3 Specifications of the test fuels

	Diesel	CNG
Chemical formula	C ₁₇ H ₃₄	CH ₄
Molar mass (g/mol)	238	16
Carbon content (%)	85.7	75
Hydrogen content (%)	14.3	25
Cetane number	40-50	-
Octane number	-	>120
Autoignition temperature (K)	483	853
Stoichiometric air/fuel mixing ratio	14.7	17.16
Lower heat value (kJ/kg)	42500	47140
Liquid density (kg/m ³)	831	465

Table 4 Uncertainty values of performance and emission response parameters

Response parameters	Uncertainty
Torque (Nm)	± %0.25
Pressure	± %0.6
BSFC	± %1.38
Indicated thermal efficiency (%)	± %1.16
UHC (ppm)	± %1.2
CO (% hacim)	± %1.6
NO(ppm)	± %2.3
Smoke(%)	± %1.9

Table 5 Independent variables levels

Independent variables	Codes	Level		
		-1	0	+1
Engine load (Nm)	A	50	75	100
CNG ratio (%)	B	0	40	80

Table 6 ANOVA results

Response	Model			Engine load			CNG ratio		
	F-value	P-value	Remarks	F-value	P-value	Remarks	F-value	P-value	Remarks
Imep	20.86	0.002	Significant	42.59	0.0013	Significant	0.0304	0.8683	No tsignificant
Thermal efficiency	7.26	0.0221	Significant	0.0213	0.8897	Not significant	9.54	0.0272	Significant
BSFC	2623.01	<0.0001	Significant	1863.79	<0.0001	Significant	0.1759	0.6923	Not significant
COV _{imep}	308.2	<0.0001	Significant	7.92	0.0374	Significant	1067.78	<0.0001	Significant
CA10	9.38	0.0127	Significant	0	1	Not significant	3.09	0.1392	Not significant
CA 50	11.38	0.0083	Significant	2.14	0.2029	Not significant	10.38	0.0234	Significant
Combustion duration	7.67	0.0197	Significant	6.25	0.054	Not significant	9.77	0.0261	Significant
Carbon monoxide	54.54	0.0002	Significant	24.26	0.0044	Significant	4.26	0.0941	Not significant

UHC	38.41	0.0005	Significant	11.87	0.0183	Significant	43.09	0.0012	Significant
NO _x	28.84	0.0009	Significant	29.56	0.0029	Significant	17.83	0.0083	Significant
Smoke	863.22	<0.0001	Significant	242.83	<0.0001	Significant	576.91	<0.0001	Significant

Table 7 Response R_2 and adj. R_2 value results

Response	R_2	Adj. R_2	Difference
Imep	0.9669	0.9205	0.0464
Thermal efficiency	0.9104	0.7850	0.1254
BSFC	0.9997	0.9993	0.0004
COV _{imep}	0.9977	0.9945	0.0032
MRR	0.9873	0.9695	0.0178
CA10	0.9292	0.8301	0.0991
CA 50	0.9409	0.8582	0.0827
Combustion duration	0.9148	0.7956	0.1192
Carbon monoxide	0.9871	0.9690	0.0181
Hydrocarbon	0.9817	0.9562	0.0255
NO _x	0.9758	0.9420	0.0338

Table 8 Optimization parameters and results

Parameter	Approach	Limits		Optimized input and response parameters	Unit
		Lower	Upper		
A-Engine load	In range	50	100	68.364	Nm
B-CNG ratio	In range	0	80	2.864	%
IMEP	Maximize	3.21	6.03	4.487	bar
ITE	Maximize	24.95	39.26	39.3	%
BSFC	Minimize	247.9	384.4	255.5	g/kWh
COV _{imep}	In range (1-6)	3.14	20.74	3.343	%
CA10	None	1.08	4.32	1.45	°CA
CA50	None	15.48	23.04	18.415	°CA
Combustion duration	None	54.36	84.6	70.31	°CA
CO	Minimize	0.061	1.86	0.247	%
HC	Minimize	110	498	191.566	ppm
NO	Minimize	468	1036	579.538	ppm
Smoke	Minimize	0.02	4.89	1.393	m ⁻¹

Nomenclature

BSFC	Brake specific fuel consumption	k	Polytropic index
BTDC	Before Top Dead Center	n	Engine speed
CA	Crank angle	NO _x	Nitrogen oxides
CA10	Crank angle location of 10% accumulated HRR (°CA)	P	In-cylinder pressure
CA50	Crank angle location of 50% accumulated HRR (°CA)	Q	Heat release rate
CCD	Central composite design	RCCI	Reactivity controlled compression ignition
CD	Combustion duration	RI	Ringling intensity
CI	Compression ignition	RSM	Response surface method
CNG	Compressed natural gas	SOC	Start of combustion
CO	Carbon monoxide	θ	Crank angle

COV _{imep}	Indicated mean effective pressure variance coefficient	T_g	In-cylinder temperature
DC	Direct current	T_w	Cylinder wall temperature
DEE	Diethyl ether	UHC	Unburned hydrocarbon
IMEP	Indicated mean effective pressure	V	Cylinder volume
ITE	Indicated thermal efficiency	WTCH	World Harmonized Transient Cycle